



# An on-demand plant-based actuator created using conformable electrodes

Wenlong Li<sup>1,2</sup>, Naoji Matsuhisa<sup>1</sup>, Zhiyuan Liu<sup>1</sup>, Ming Wang<sup>1</sup>, Yifei Luo<sup>1</sup>, Pingqiang Cai<sup>1</sup>, Geng Chen<sup>1</sup>, Feilong Zhang<sup>1</sup>, Chengcheng Li<sup>1</sup>, Zhihua Liu<sup>1</sup>, Zhisheng Lv<sup>1</sup>, Wei Zhang<sup>1</sup> and Xiaodong Chen<sup>1</sup>✉

**Owing to their adaptive interfacial properties, soft actuators can be used to perform more delicate tasks than their rigid counterparts. However, traditional polymeric soft actuators rely on energy conversion for actuation, resulting in high power input or slow responses. Here we report an electrical plant-based actuator that uses a conformable electrical interface as an electrical modulating unit and a Venus flytrap as an actuating unit. Using frequency-dependent action-potential modulation, accurate on-demand actuation is possible, with response times that can be tuned to 1.3 s and a power input of only 10<sup>-5</sup> W. The actuator can be wirelessly controlled using a smartphone. It can also be installed on a range of platforms (including a finger and a robotic hand) and can be used to grasp thin wires and capture moving objects.**

Soft actuators with a high degree of compliance are of potential use in delicate task settings and unstructured environments<sup>1–5</sup>. Various soft actuators have been developed based on fluidic/pneumatic elastomers<sup>6</sup>, shape memory<sup>7</sup> and electroactive<sup>8</sup> polymers. However, energy conversion is required in these artificial polymeric materials for shape changing or mechanical movement, leading to a high power input or slow response. Alternatively, biohybrid actuators using contractile muscles<sup>9,10</sup> or mobile cells<sup>11,12</sup> require minimal power input, but tissues and cells are complicated to prepare and their actuation is relatively unpredictable<sup>13,14</sup>.

Plants have a range of sophisticated capabilities<sup>15</sup>, including behavioural plasticity<sup>16</sup>, network-like communication<sup>17</sup>, an ability to learn and memorize<sup>18</sup>, sophisticated morphogenesis<sup>19,20</sup> and intricate functional microstructures<sup>21,22</sup>. The Venus flytrap (*Dionaea muscipula*), in particular, is a thigmonastic plant that can lock insects in its lobes<sup>23</sup>; touches on its upper epidermis generate action potentials (APs) that can trigger rapid flytrap closing<sup>24,25</sup> (Supplementary Figs. 1–3). Because flytrap actuation is internally triggered by electrophysiological signals<sup>26</sup>, artificial interference with the plant's electrophysiology through external electricity could, in theory, modulate its actuation behaviour.

To electrically interfere with a plant's electrophysiology, two key challenges exist. The first is to create a physical interface allowing communication with the plant. Such an interface should be integrated on the plant surface without affecting the plant movement or physiology. Unlike human skin, a plant's surface is protected by a hydrophobic waxy cuticle layer, making the attachment of thin-film electronic devices difficult. The second challenge is to achieve effective communication with the plant. Currently, no standardized electrical communication methods with plants exist. Electrostimulation-induced flytrap closure has been achieved, but the mechanism remains unclear, and accurate modulation has not been possible<sup>27,28</sup>.

In this Article, we show how the thigmonastic response of a Venus flytrap can be used to build on-demand actuator devices. Plant-conformable electrodes were developed as a physical interface,

and frequency-dependent action potential modulation was explored as an electrical communication protocol. The resulting plant-based actuator (termed as a phytoactuator) uses Venus flytrap lobes as the actuating unit and conformable electrodes as the electrical modulating unit (Fig. 1a). The electrical phytoactuator requires no energy conversion and is power efficient (input voltage and power as low as 1.5 V and 10<sup>-5</sup> W, respectively). It is also responsive (response time can be modulated to around 1.3 s), compatible with complementary metal-oxide-semiconductor (CMOS)-based electronics (easily accessed using a Wi-Fi module for wireless smartphone control), modular and installable on various platforms (can be isolated from plant stem and integrated on a finger, robotic hand or manipulator), and capable of capturing fine and moving objects.

## Conformable electrodes for plant electrical modulation

To modulate the flytrap's electrophysiology, plant electrodes that can either detect electrical signals from the plant or deliver an electrical field to the plant are needed<sup>29</sup>. Traditional electrode protocols (Supplementary Fig. 4) adopted by plant biologists include intracellular methods (glass microelectrodes<sup>30</sup> or aphid-stylet-based electrodes<sup>31</sup>) and extracellular methods (inserted wire electrodes<sup>32</sup> or surface Ag/AgCl–agar electrodes<sup>23,33</sup>). While suitable for the fundamental studies of plants, these methods cannot be implemented in a bioelectronics device because they are invasive, easily detached from plants and require complicated setup procedures. While a vapour printing method of a conductive polymer on the plant surface was recently reported, the harsh printing conditions (slight heating and diluted acid solution washing) makes it unsuitable for most sensitive and fragile plants<sup>34</sup>. Electrodes for the phytoactuator devices should ideally be non-invasive, compliant with the plant morphology and movement, miniaturized and portable, and effective at the ionic–electronic current transduction. Achieving this requires the electrode to conform to the surface of the plant (Supplementary Fig. 5). However, this is challenging because the plant epidermis has a waxy cuticle layer containing rough microstructures<sup>22</sup>.

<sup>1</sup>Innovative Center for Flexible Devices (iFLEX), Max Planck–NTU Joint Lab for Artificial Senses, School of Materials Science and Engineering, Nanyang Technological University, Singapore, Singapore. <sup>2</sup>NTU Institute for Health Technologies, Interdisciplinary Graduate Programme, Nanyang Technological University, Singapore, Singapore. ✉e-mail: [chenxd@ntu.edu.sg](mailto:chenxd@ntu.edu.sg)

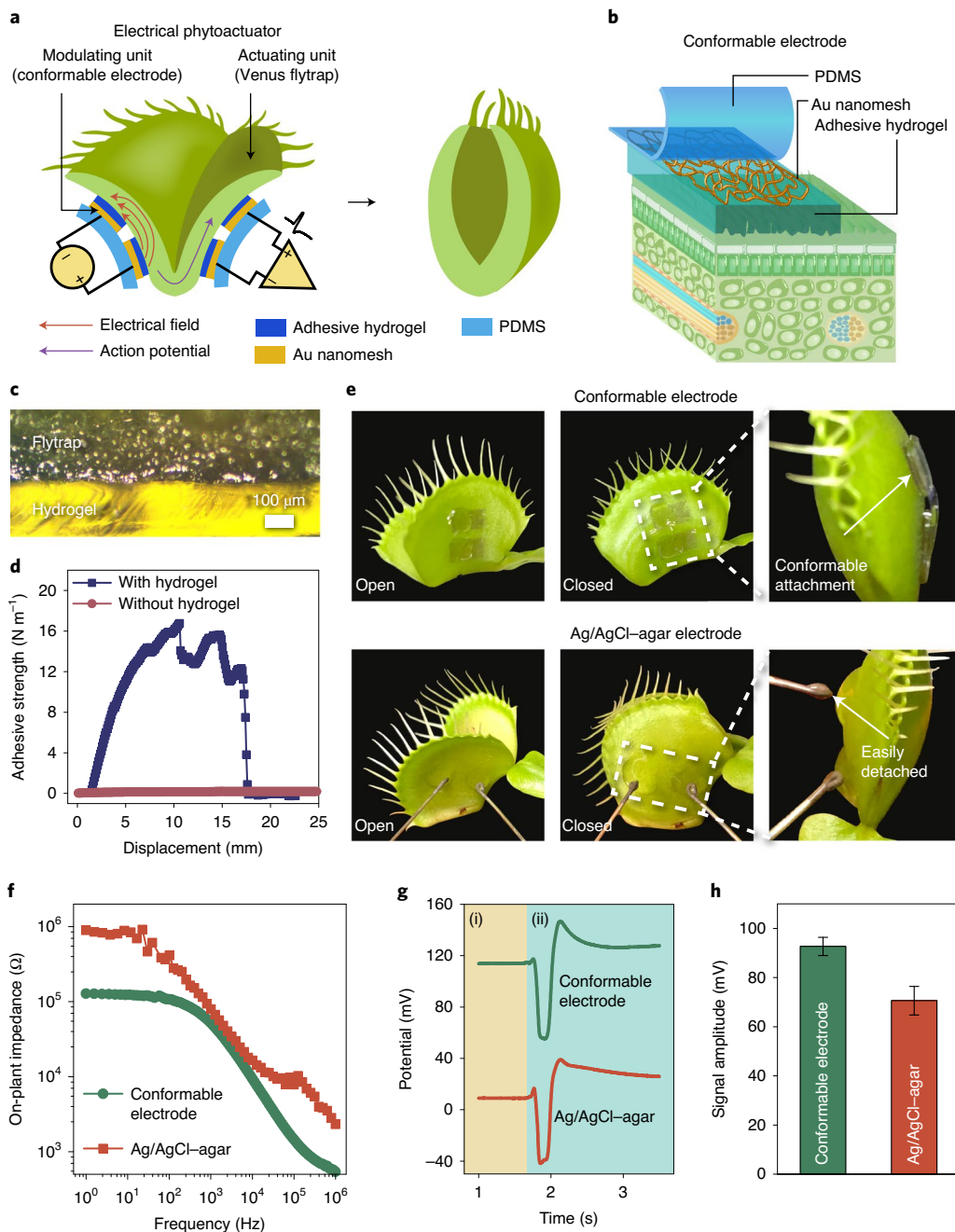


**Fig. 1 | Electrically modulated biohybrid phytoactuator.** **a**, Left: schematic of the phytoactuator. Venus flytrap is the actuating unit, and conformable electrodes form the modulating unit. The conformable electrode system can deliver an electric field to the flytrap and simultaneously measure the electrical signals, that is, APs, from the flytrap. Right: schematic showing a closed flytrap lobe after electrical actuation. **b**, Schematic of the conformable electrode attached to the surface of a leaf. **c**, Optical micrograph of a cross-section of the flytrap and adhesive hydrogel shows the conformable attachment of the hydrogel. **d**, Adhesive strength of the conformable electrode with hydrogel on the plant surface compared with that without hydrogel. **e**, Photographs of a conformable electrode (top row) and traditional Ag/AgCl–agar electrode (bottom row) on the flytrap epidermis. Conformable electrodes remain attached to the flytrap epidermis in both open (top left) and closed (top middle) state. The zoomed-in views (right) show that the conformable electrodes conform to the epidermis in the closed state and the Ag/AgCl–agar electrodes (brown rods) attach to the flytrap epidermis in the open state (bottom left) but easily detach in the closed state (bottom middle and bottom right). **f**, A conformable electrode has a smaller on-plant impedance than the Ag/AgCl–agar electrode. **g**, Representative AP signals obtained from the conformable electrode and Ag/AgCl–agar electrode. Electrical signals before (i) and after (ii) the mechanical touch. **h**, Signal amplitude analysis of nine AP signals shows conformable electrodes give a larger signal amplitude than the Ag/AgCl–agar electrodes. Error bars are s.d. from nine samples.

Our conformable electrode resolves these issues by employing a soft and adhesive hydrogel layer as the plant-contacting layer and gold (Au) nanomesh on polydimethylsiloxane (PDMS) as the electronic transduction layer (Fig. 1b). The conformable electrode

system can simultaneously deliver customized modulating electricity to and detect electrical signals from the plant, offering a way to monitor the electrophysiological signals of the plant during electrical modulation (Fig. 1a). The conformable electrode is also

non-invasive in that it only senses or induces capacitive currents in the plant tissue separated by the cuticle layer, while no electrochemical reaction takes place between the plant and the electrode. The adhesive hydrogel is prepared from the thermo-polymerization of acrylic acid monomers with 10 mM KCl ionic additive<sup>35</sup>. The adhesive poly(acrylic acid) hydrogel film allows the electrode to adhere and conform to the plant surface (Fig. 1c). In a 90° peel-off test from the plant surface, electrodes with a hydrogel layer recorded an adhesive strength of 15.6 N m<sup>-1</sup>, while electrodes without the hydrogel showed negligible adhesion (Fig. 1d). This confirms that an adhesive interface between the hydrogel layer and the plant surface exists. The hydrogel layer is also ionically conductive, stretchable, biocompatible and transparent enough for normal chlorophyll activity to occur (Supplementary Figs. 6 and 7).

For the electronic conduction layer, we synthesized an Au nanomesh film using wet chemistry (Supplementary Figs. 8–10)<sup>36,37</sup> and transferred the two-dimensional intertwined Au nanomesh network that formed at the water surface onto PDMS. The Au nanomesh–PDMS film was sufficiently transparent for effective light absorption by the plant (Supplementary Fig. 11). The film was highly stretchable, stable upon 50% strain cycling and remained conductive even at 135% strain (Supplementary Fig. 12). The interfacial current transduction between the Au nanomesh and adhesive hydrogel is also highly efficient (Supplementary Fig. 13), as the interfacial admittance of the Au nanomesh with the adhesive hydrogel is higher than those of carbon nanotube (CNT), silver nanowire (AgNW) and aluminium film. Further, the conformable electrode is only around 4.9 mg, much lighter than a flytrap lobe (around 228 mg), presenting a negligible weight effect when attached to the flytrap (Supplementary Fig. 14 and Supplementary Table 1). These results demonstrate that our conformable electrodes, which are conductive, transparent, lightweight, easy to apply and conform well to plant surfaces, form a promising biocompatible electrical interface for sensing and modulating the plant's electrophysiology. They also provide a new avenue for the development of plant bioelectronics based on biocompatible adhesive hydrogels.

Compared with the current gold standard set by non-invasive Ag/AgCl–agar electrodes used for surface potential measurements in plants<sup>12,13</sup>, our conformable electrodes attached better to the flytrap lobe from the open to the closed state (Fig. 1e). This firm adhesion ensures the continuous and accurate sensing of electrical signals and the delivery of modulating electricity; further, this is necessary because the flytrap has a fast nastic response. As shown in Fig. 1e, Ag/AgCl–agar electrodes can easily detach from the leaf epidermis during flytrap closure. On-plant impedance measurements show that the firm adhesion of the conformable electrodes lowers the contact impedance (Fig. 1f). Conformable electrodes showed an impedance of around 300 k $\Omega$  compared with around 1 M $\Omega$  for Ag/AgCl–agar electrodes at low frequencies (1–10 Hz). The lower on-plant impedance of conformable electrodes also agreed well with the AP signal measurements. The shapes of the AP signals obtained from both conformable electrodes and Ag/AgCl–agar electrodes were comparable (Fig. 1g and Supplementary Figs. 15 and 16). An analysis of nine AP signals (Fig. 1h) further verified that the conformable electrodes (92.7  $\pm$  3.7 mV) presented a larger signal amplitude than the Ag/AgCl–agar electrodes (70.6  $\pm$  5.8 mV). These results show that our conformable electrodes are well suited for electrical interfacing with plants.

### Electrical modulation of the flytrap

Using the conformable electrodes, we show that each mechanical touch induces one AP and it takes two successive APs to close the flytrap lobes (Supplementary Fig. 17), which agrees with the literature<sup>26</sup>. The time interval between the two touches, however, must not be longer than 60 s for the lobes to close; intervals longer than 60 s will not close the lobes (Supplementary Fig. 18). These results

confirm that mechanical perception is transduced into an electro-physiological signal in the form of the AP and that the flytrap is capable of memory—it can register the first AP and compute two successive APs within 60 s to initiate lobe actuation (Supplementary Fig. 19)<sup>26</sup>.

To electrically actuate the flytrap, we attached a pair of conformable electrodes on each of the two lobes (Fig. 2a). One pair of electrodes is for stimulation and the other pair is for acquiring potential signals. Flytrap actuation is measured by a normalized lobe-edge distance,  $y/y_0$ , where  $y$  refers to the edge distance of the two lobes and  $y_0$  is the initial edge distance before flytrap actuation. Upon stimulation by a direct current (d.c.) of 3 V, one AP was immediately generated, followed by a series of APs during a stimulation period of 40 s (Fig. 2b,c). Interestingly, similar to the mechanical stimulation of a flytrap shown in Supplementary Fig. 17, electrical stimulation also induces lobe closure after the second AP (Fig. 2c), indicating that two APs are needed for electrical flytrap actuation. Different d.c. voltage stimulations from 0.5 to 3.0 V show a threshold voltage of around 1.5 V (Fig. 2d and Supplementary Fig. 20). A series of autonomous APs were observed for stimulations  $\geq 1.5$  V, whereas no APs were seen for those stimulated at  $< 1.5$  V (Fig. 2e). Indeed, we found that almost all the electrical actuation cases were linked with the appearance of a second AP. To verify this, the response time (defined as the time interval between the start of stimulation and start of flytrap actuation, as extracted from the  $y/y_0$  data) and first two-AP interval (defined as the time interval between the first and second AP during d.c. stimulation, as extracted from the potential signal data) were compared (Fig. 2f). The linear fitting of the response time versus the first two-AP interval showed a strong correlation between the two, with an R-squared value of 0.986, indicating the important role of the two APs in electrical flytrap actuation. Moreover, simultaneous current density measurements also displayed spikes that coincided with the appearance of APs for stimulating voltages  $\geq 1.5$  V, demonstrating that the increase in the plant tissue conductance is related to AP generation (Supplementary Fig. 21). Changing the electrode geometry and position shows no distinguishable differences in flytrap actuation under d.c. stimulation (Supplementary Figs. 22 and 23), indicating an isotropic presence of excitable tissues in the flytrap.

Although the phenomenon of electrically induced flytrap closure and a threshold of 1.5 V was reported in the literature, previous studies on the electrical stimulation of flytrap used a charge-injection capacitor or a function generator by invasive silver wire electrodes, and the electrically induced flytrap closure was attributed to direct charge injection into the flytrap motor cells<sup>27,28</sup>. Our non-invasive conformable electrode system avoided direct charge injection into the flytrap tissue but only induced a capacitive current flow inside the plants. Moreover, simultaneous potential signal and current density measurements confirm the generation of APs. Our results suggest that flytrap closure by electrical stimulation is similar to mechanical stimulation in that it relies on two-AP memory and computation.

It is further noted that the AP intervals—the time duration between two autonomous APs induced by d.c. stimulation—are random (Fig. 2e and Supplementary Fig. 24). However, an analysis of 376 AP intervals in d.c. stimulation showed that a minimum limit of 1.2 s exists (Fig. 2g). Such a limit resembles the refractory period of neurons, where it is defined as the time during which another AP cannot be generated due to the generation of the first AP. The AP interval limit in our experiment suggests that the refractory period of the flytrap is probably around 1.2 s, which is much longer than the refractory period of neurons (a few milliseconds). To further verify the AP refractory period in the flytrap, we mechanically stimulated the flytrap twice within 0.3 s and found that it remained open even after two touches, indicating that two APs cannot be generated within the refractory period (Supplementary Fig. 18). In contrast

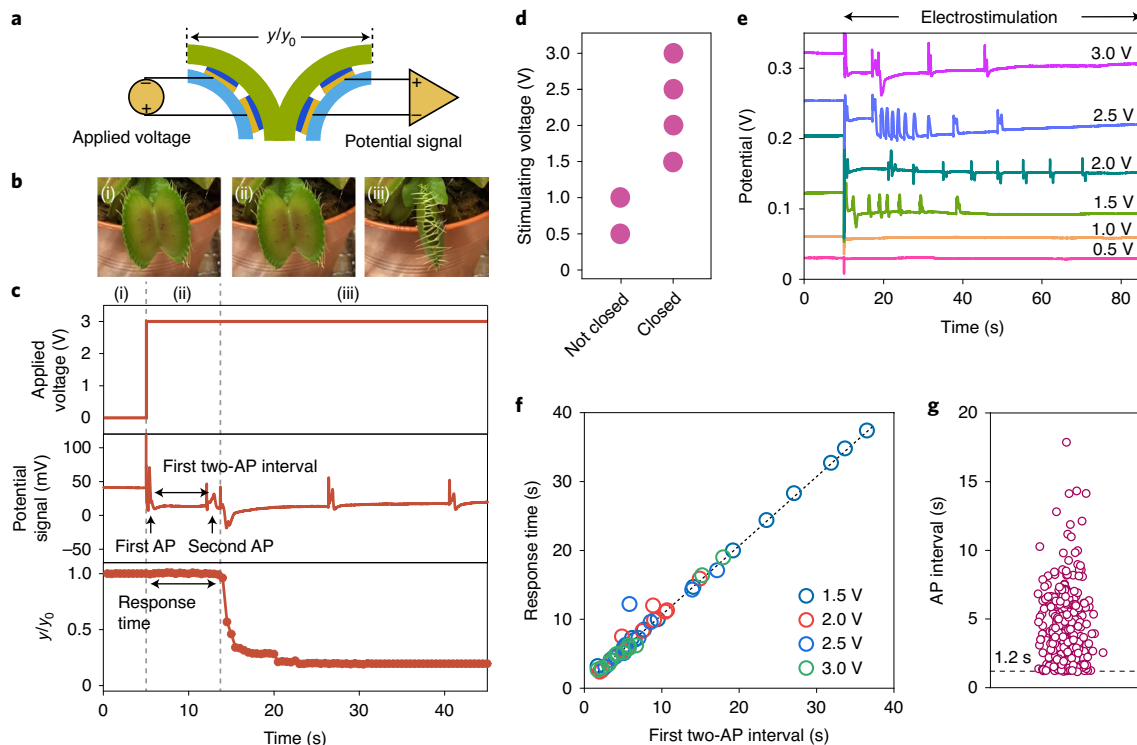


**Fig. 2 | Flytrap stimulation by d.c. voltage.** **a**, Schematic showing a pair of conformable electrodes attached to each flytrap lobe. The left lobe is stimulated by the applied voltage (3 V d.c.) and potential signals are acquired from the right lobe. Lobe closing is determined by the lobe-edge distance,  $y/y_0$ , where  $y$  is the distance at any time and  $y_0$  is the initial distance before actuation. **b**, Photographs of the flytrap stimulated by 3 V d.c. **c**, Simultaneous recording of the potential signal and  $y/y_0$  when a 3 V d.c. voltage is applied. Upon applying this voltage, the first AP is immediately formed, followed by a series of APs. The flytrap closes after the second AP. **d**, Flytraps stimulated at different voltages show a threshold voltage of 1.5 V for phytoactuation. **e**, Potential signals acquired from conformable electrodes over 75 s at different d.c. stimulating voltages. **f**, Correlation of the response time and first two-AP interval for different d.c. stimulations, confirming the two-AP mechanism in electrical stimulation. Each voltage group was repeated for 12 samples. **g**, AP interval analysis in AP series generated by d.c. stimulations, indicating the refractory period of around 1.2 s in the flytrap. The black dashed line indicates a reference for 1.2 s. The number of AP intervals analysed: 376.

to the previous estimation of the flytrap's AP refractory period (3–5 s) induced by light<sup>38</sup>, our results show the direct experimental proof of the flytrap's AP refractory period in electrical stimulation. In summary, the two-AP mechanism and the refractory period in flytrap during electrical stimulation provide a biological basis for developing plant communication protocols to realize accurate phytoactuation.

While d.c. stimulation above 1.5 V can induce a series of APs for flytrap closure, the appearance of the second AP, and therefore the response time for flytrap closure, is usually random (Supplementary Fig. 20). When the electrical stimulus was changed from d.c. to a square wave, the actuation behaviour could be modulated faster and more accurately (Supplementary Fig. 25). Under a stimulating frequency of 0.1 Hz, the response time generally takes  $4.7 \pm 1.4$  s (Fig. 3a). Increasing the frequency to 0.5 Hz significantly reduces the response time to  $1.8 \pm 0.4$  s. However, beyond 0.5 Hz, the decrease in the response time plateaus. At 2 Hz, the response time decreases only to  $1.3 \pm 0.1$  s. To understand how the stimulating frequency modulates the response time, we registered potential signals with two conformable electrode pairs during square-wave stimulation. A square wave contains a rising edge and a falling edge, each of which induced one AP (Fig. 3b). In contrast, a 'dead' flytrap showed no rising-edge and falling-edge AP during square-wave modulation (Supplementary Fig. 26). As a result, one square wave can accumulate exactly two APs for flytrap actuation, explaining the reason for the frequency-dependent modulation of the response time. However, by converting the stimulating frequency ( $f$ ) to the rising-falling

edge interval ( $t$ ) using the expression  $t = 1/(2f)$ , the response time is predicted as 0.25 s at 2 Hz, which significantly deviates from the experiments. Instead of approaching 0 s as the frequency increases, the response time approached  $1.3 \pm 0.1$  s. Together with Fig. 2g showing a refractory period of 1.2 s, these results demonstrate that the frequency modulation is limited by the refractory period, and therefore, two APs cannot be generated within this period. More importantly, the convergence of response time from random under d.c. stimulation to the refractory period limit under 2 Hz frequency modulation indicates that most flytraps share a similar refractory period. This is the biological basis for the accurate modulation of flytraps on different samples. To further explain AP generation in d.c. stimulation and frequency-dependent modulation, we propose a qualitative hypothesis that involves the capacitive charging of the excitable membrane of the flytrap using an external electrical field. A detailed discussion is provided in Supplementary Fig. 27.

The fact that plants usually grow in pots makes the practical applications difficult when converting plants into bioelectronic devices. For better device mobility and portability, we explored the modular property of the Venus flytrap. The flytrap lobes were isolated from its petiole (the supportive connection to the roots) and the cut was sealed with an Ecoflex elastomer to prevent tissue dehydration. Interestingly, the modular flytrap lobes continued to display good electrical actuation for up to one day. For more prolonged survival, better methods to prevent dehydration must be explored. As shown in Fig. 3c and Supplementary Fig. 28, the response time of the modular flytrap ( $16.2 \pm 10.4$  s) was retarded compared with the

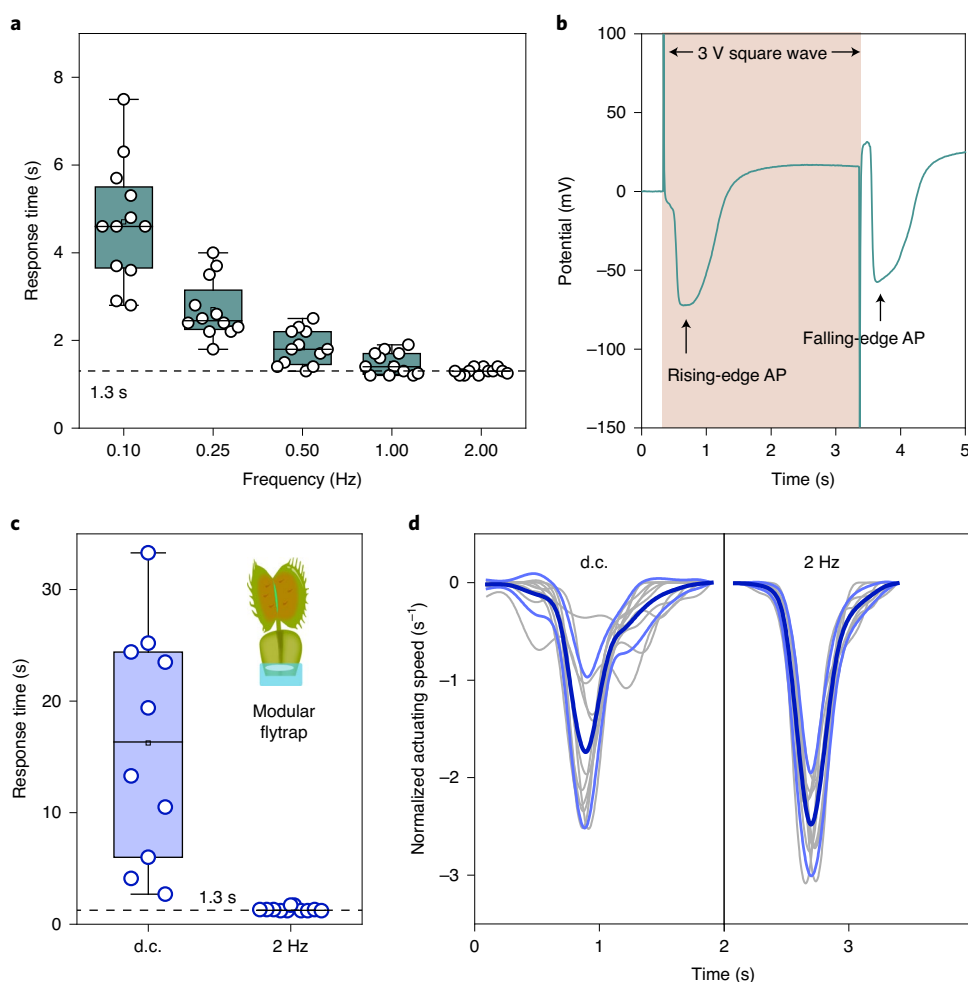


**Fig. 3 | Frequency-dependent modulation of flytrap actuation.** **a**, Modulation of the response time of the flytrap at different frequencies. The black dashed line indicates a reference for 1.3 s. The boxes show the upper and lower quartiles, the open square in the boxes is the mean, the middle line is the median, the whiskers represent 1.5 times the interquartile range and the open circles show the data points. Each frequency group was repeated for 12 samples. **b**, Potential signal measurement—when stimulated by a 3 V square wave—shows that one AP forms immediately following each rising edge and falling edge of the square wave. **c**, Direct current modulation of the modular flytraps shows a large response time ( $16.2 \pm 10.4$  s), while 2 Hz square-wave modulation can approach the response-time limit of 1.3 s. The inset shows a schematic of the modular flytrap. The black dashed line indicates a reference for 1.3 s. The boxes show the upper and lower quartiles, the open square in the boxes is the mean, the middle line is the median, the whiskers represent 1.5 times the interquartile range and the open circles show the data points. Each sample group was repeated for ten samples. **d**, Actuating kinetics of the modular flytraps show accelerated actuating kinetics by 2 Hz square-wave modulation. The normalized actuating speed was obtained by taking the first-order derivative of the  $y/y_0$  data shown in Supplementary Fig. 28. The dark blue line represents the mean and the light blue line represents the s.d. of the normalized actuating speeds for ten samples. The overlapping grey lines represent the raw data.

flytrap in pots ( $6.8 \pm 5.2$  s). However, the 2 Hz square-wave modulation can eliminate such retardation, approaching the response-time limit of 1.3 s. Further, as shown in Fig. 3d, the 2 Hz square-wave modulation can increase the normalized actuating speed (maximum value,  $-2.8 \pm 0.4$  s $^{-1}$ ) compared with d.c. modulation (maximum value,  $-2.0 \pm 0.8$  s $^{-1}$ ). These results show that modular flytraps can work well without any actuation performance loss using frequency modulation, providing the possibility to install the phytoactuator, in principle, on any other devices or platforms.

Our electrical phytoactuator with a response time of 1.3 s is faster than most of the recent soft electrical actuators (Supplementary Fig. 29 and Supplementary Tables 2 and 3). Further, the phytoactuator only requires a voltage input of 1.5 V at a power consumption of  $10^{-5}$  W, which is 4–5 orders of magnitude smaller than traditional devices (1.0–0.1 W). The phytoactuator has such a fast response time and low power consumption because actuation is completed by the flytrap itself. Electrical energy serves only as a stimulus and is not

converted to mechanical energy for actuation. This feature presents an out-of-the-box strategy for developing actuator devices based on natural resources such as plants; our task is to find ways to interface with and modulate the various intelligent systems found in nature. However, one issue related to reversibility remains. Although the closure process can be accurately modulated, it takes hours to naturally reopen the flytrap. Electrical modulations showed no effect in accelerating the flytrap reopening. As the closing process involves a fast release of hydroelastic energy between the outer and inner layers of the flytrap<sup>39</sup>, accelerating the re-storage of hydroelastic energy between the two layers may accelerate flytrap reopening.

### An on-demand electrical phytoactuator

In light of the increasing dependence on the cyber interface for human–environment interactions, we tested the modular flytraps by implementing a smartphone-controllable phytoactuator (Fig. 4a,b, Supplementary Fig. 30 and Supplementary Video 1). Because our

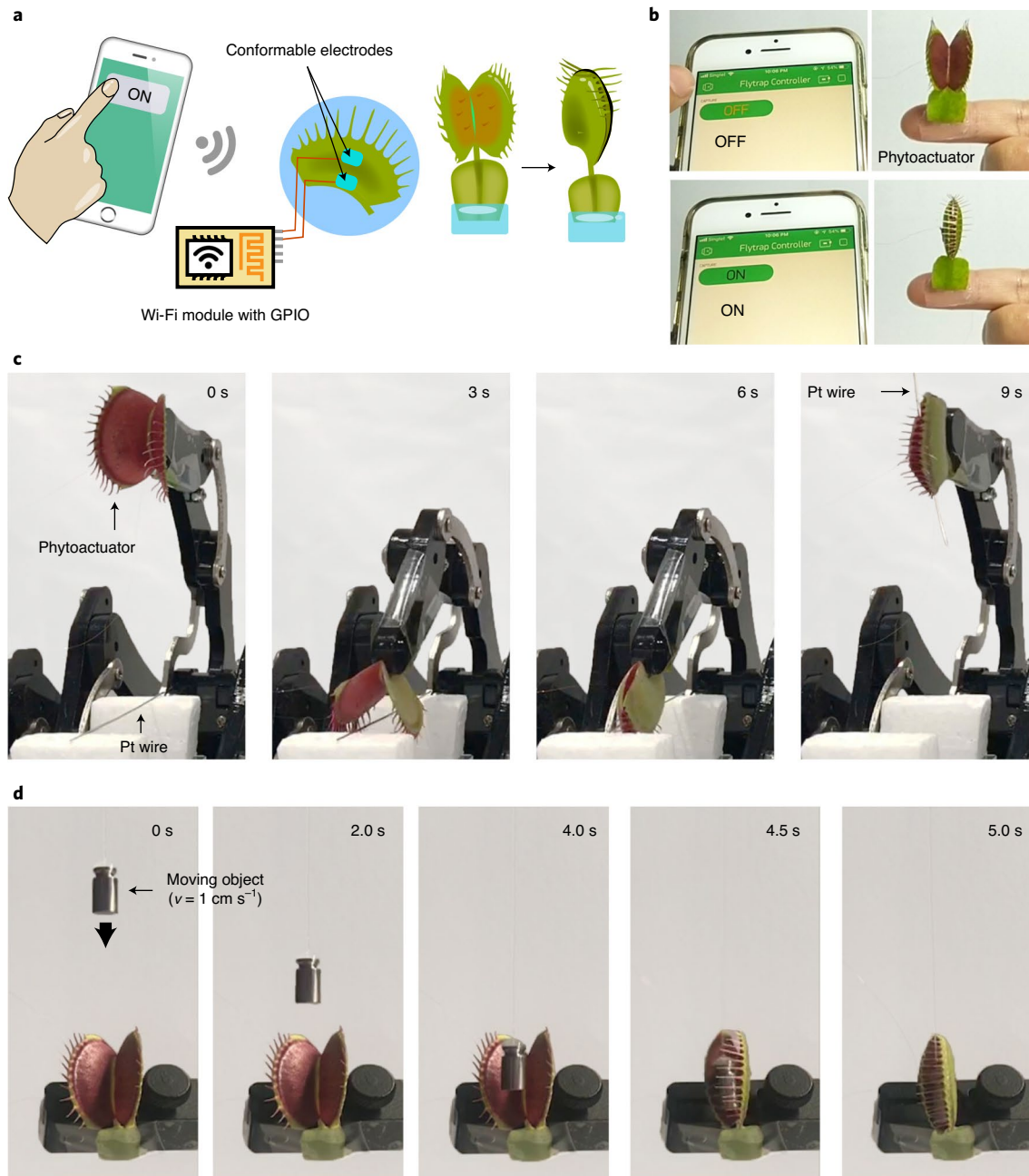


**Fig. 4 | Integration of a modular electrical phytoactuator with other platforms.** **a**, Schematic showing the implementation of a smartphone-controllable phytoactuator. An 'ON' command from the smartphone application is sent via the Internet to a Wi-Fi module (ESP8266) with a GPIO terminal. The Wi-Fi module then sends a 3.3 V voltage to the conformable electrodes, which triggers flytrap closure. **b**, Photograph of the phytoactuator as controlled by a smartphone. **c**, Photographs showing the integration of the phytoactuator with a robotic hand enables the hand to perform delicate tasks such as grasping a thin (0.5 mm diameter) Pt wire. **d**, Photographs showing that the accurate modulation of the response time of the flytrap allows the phytoactuator mounted on a manipulator to capture a moving object (1 g weight) at a velocity,  $v$ , of  $1 \text{ cm s}^{-1}$ .

phytoactuator has a low threshold voltage of 1.5 V, it is accessible to cyberspace through miniaturized electronic systems (such as a typical Wi-Fi chip with an output voltage of 3.3 V). As shown in Fig. 4a,b, the command given by the user through a smartphone application is sent via the Internet to a Wi-Fi module (ESP8266) containing a general-purpose input/output (GPIO) terminal. Upon receiving the command, the Wi-Fi module sends a 3.3 V electrical output to the conformable electrodes, which initiates the actuation of the flytrap lobes. This experiment shows that the modular phytoactuator can communicate with CMOS-based electronics on demand via our conformable electrodes. Compared with the

dedicated electrostimulation setups in the literature (such as low-noise function generator, optocoupler isolation and signal conditioning circuits)<sup>27,28</sup>, the smartphone trigger is based on a Wi-Fi chip that is lightweight (around 10 g), programmable and accessible by the Internet. This presents a possibility of connecting plants into the cyberspace.

While conventional robots are good at performing repetitive tasks in well-structured and well-defined environments, they are less efficient when it comes to handling undefined objects in changing environments. For example, the robotic hand would typically struggle to pick up small and fine objects. In contrast, with the

hair-like cilia projections lining the lobe edge, the flytrap is capable of grasping and tightly locking small insects such as mosquitoes. We combined the positioning capabilities of a robotic hand with the grasping abilities of the phytoactuator by attaching the isolated phytoactuator on a robotic hand. After carefully positioning the robotic arm, the flytrap was activated through the smartphone as before, causing the lobes to close and pick up a thin (0.5 mm diameter) platinum (Pt) wire (Fig. 4c and Supplementary Video 1). Because the response time of our phytoactuator can be accurately modulated, we show that it can also be used in dynamic environments to capture moving objects (Fig. 4c and Supplementary Video 1). If the kinetic information of the moving object is known, the capturing task can be implemented by buffering the response time in advance. For example, for a 1 g weight of object falling at a speed of  $1 \text{ cm s}^{-1}$ , the phytoactuator mounted on a manipulator can be modulated to capture the object as it falls through the lobes.

## Conclusions

We have reported an electrical phytoactuator that uses the lobe of a Venus flytrap as the actuating unit and conformable electrodes as the modulating unit. The conformable electrodes were used to modulate the flytrap's electrophysiology and perform on-demand actuation of the lobes. We also showed that the phytoactuator can be combined with a robotic arm to pick up a fine wire and independently modulated to capture a moving object. Our conformable electrical interface could be used as the basis for a range of plant studies and developments of plant bioelectronics. In particular, the ability to interfere with a plant's electrophysiology through external electrical stimulation opens new possibilities for building plant communication protocols. Moreover, as illustrated in our work, plants are modular, and they can be isolated and installed on a variety of platforms. Integrated with current soft electronics<sup>40–42</sup> or plant-based electronics<sup>43–45</sup>, such modularity could potentially be used to build various plant-based robots, sensors, memristors, ionic circuits and plant healthcare devices.

## Methods

**Fabrication of conformable electrodes.** The Au nanomesh film was synthesized as previously reported<sup>36,37</sup>. Briefly, 4.8 mg of gold(III) chloride trihydrate ( $\text{HAuCl}_4 \cdot 3\text{H}_2\text{O}$ ; Sigma-Aldrich) was dissolved in 25 ml deionized water. The  $\text{HAuCl}_4$  solution was poured in a 250 ml glass beaker and stirred at 400 r.p.m. and  $5^\circ\text{C}$ . Subsequently, 1.2 mg of sodium borohydride ( $\text{NaBH}_4$ ; Fluka Analytical) was dissolved in 25 ml deionized water as a reduction agent. The  $\text{NaBH}_4$  solution was slowly added to the  $\text{HAuCl}_4$  solution drop by drop, while the bath temperature was kept at  $5^\circ\text{C}$  and the stirring rate was kept at 400 r.p.m. As  $\text{NaBH}_4$  was added, the solution changed to the red wine colour. After adding  $\text{NaBH}_4$ , 100 ml toluene (VWR Chemicals) was added to the mixed solution and the solution was stirred at 600 r.p.m. and  $5^\circ\text{C}$  for 15 min. Then the solution was rested in the ambient condition for another 30 min. There would be obvious layer separation, with toluene at the top layer and a dark reddish aqueous solution at the bottom layer. Toluene was removed; after thorough evaporation of toluene residuals, an Au nanomesh film was formed on top of the water surface. A PDMS film was prepared by mixing SYLGARD 184 silicone elastomer base and a curing agent at a ratio of 10:1, spin coated on a silicon wafer at 800 r.p.m. for 60 s and cured at  $80^\circ\text{C}$  for 5 h. The PDMS film was first attached to a polyethylene terephthalate (PET) film and the PET–PDMS film was cut into the desired shape for transfer onto the Au nanomesh. The PET–PDMS film was put in contact with the Au nanomesh on top of the water surface; the contact was kept for 20 s for a complete transfer. Then the PET–PDMS–Au nanomesh film was lifted and allowed to dry at the ambient condition. The PDMS film was peeled off from the PET for further use. To fabricate a soft hydrogel–Au nanomesh–PDMS electrode, a polyacrylic acid hydrogel precursor solution was first prepared. Briefly, in 4 ml deionized water, 1 ml acrylic acid (Sigma-Aldrich), 20 mg potassium chloride (Sigma-Aldrich), 40 mg potassium persulfate (Sigma-Aldrich), 1.67 mg  $N,N'$ -methylenebisacrylamide (Sigma-Aldrich) and 40  $\mu\text{l}$   $N,N,N',N'$ -tetramethylethylenediamine (Sigma-Aldrich) were subsequently added. To make PAA hydrogel in the desired shape, a handmade PDMS mould was made first. The PDMS mould with 3 mm  $\times$  3 mm wells was put on top of the glass substrate and a PAA hydrogel precursor solution was poured into the PDMS wells. The PDMS mould was covered by a petri dish and heated in an oven at  $70^\circ\text{C}$  for 15 min. After the heating process, the hydrogel was formed in the PDMS mould and was washed with 0.1 M KCl aqueous solution for 30 min. The washed hydrogel was transferred onto the PDMS–Au nanomesh film,

forming a PDMS–Au nanomesh–hydrogel electrode. One end of the electrode was wired by a copper wire dipped in a liquid metal point (gallium–indium eutectic, Sigma-Aldrich). Ecoflex elastomer was used to seal the wiring point.

**Characterization of the synthesized Au nanomesh.** The as-synthesized Au nanomesh on the water surface was lifted by the copper grid and was allowed to thoroughly dry. The Au nanomesh sample on the copper grid was observed by field-emission transmission electron microscopy (JEOL, JEM-2100F) for studying the nanostructure and morphology. The aqueous solution of the Au nanomesh was collected and light absorption was analysed using ultraviolet–visible (UV–vis) spectroscopy (Shimadzu UV-2550 UV–vis spectrophotometer). The Au nanomesh transferred on PDMS was characterized by field-emission scanning electron microscopy (JEOL, 7600F). The Au nanomesh–PDMS film was also characterized by UV–vis spectroscopy (Shimadzu UV-2550 UV–vis spectrophotometer) for transmittance studies.

**Electrical characterization of the conformable electrodes.** The cyclability of the Au nanomesh–PDMS film ( $3 \text{ cm} \times 1 \text{ cm}$ ) was measured by a parameter analyzer (Keithley 4200) and a mechanical tester (MTS Criterion model C42). A 50% strain was applied to the film at a strain rate of  $0.2 \text{ mm s}^{-1}$  for 200 times by the mechanical tester. The resistance of the film was recorded by the parameter analyzer. The stretchability of the Au nanomesh–PDMS film ( $3 \text{ cm} \times 1 \text{ cm}$ ) was measured by the parameter analyzer and the mechanical tester. The film was stretched at a strain rate of  $0.2 \text{ mm s}^{-1}$  until rupture. The resistance of the film was recorded by the parameter analyzer. The interfacial impedance between the electronic films and hydrogel was measured by an electrochemical workstation (Zennium E, Zahner Ennium). A hydrogel film ( $1 \text{ cm} \times 1 \text{ cm}$ ) was sandwiched between two Au nanomesh–PDMS films ( $2 \text{ cm} \times 1 \text{ cm}$ ), with the Au nanomesh in contact with two sides of the hydrogel film. The impedance of the Au nanomesh–hydrogel–Au nanomesh film was measured from  $10^0$  to  $10^6$  Hz. The admittance was calculated as the reciprocal of the impedance to reflect the ease of current transduction from the Au nanomesh to the hydrogel. As control groups, AgNW and CNT on the PDMS film ( $2 \text{ cm} \times 1 \text{ cm}$ )—with conductance similar to the Au nanomesh film—and the aluminium foil were also measured with the same sandwich configuration. AgNW and CNT films were prepared by the vacuum filtration method, where AgNW and CNT were first filtrated on a filter paper and then transfer printed on a PDMS film; the conductance values of the AgNW and CNT films were tuned by the amounts of solution filtrated on the filter paper.

**Adhesive strength of hydrogel on the plant leaf surface.** The adhesive strength of the hydrogel on the plant leaf surface was evaluated by a  $90^\circ$  peel-off experiment. Briefly, the hydrogel film was synthesized with predefined dimensions of  $40.0 \text{ mm} \times 15.0 \text{ mm} \times 0.1 \text{ mm}$  on a polyimide film. The polyimide film was used as a backing layer to restrict the elongation of the hydrogel during peeling; thus, the applied force is mostly used for peeling rather than straining. On the mechanical tester, a leaf was cut into a rectangular shape and was fixed on the bottom plate of the tester with a double tape. A hydrogel with a polyimide backing was pressed onto the leaf surface, and one end was fixed with the upper gripper. The strain rate was set at  $0.2 \text{ mm s}^{-1}$ , and the hydrogel with the polyimide backing was slowly peeled off from the leaf. The plateau of force during peeling was averaged and divided by the hydrogel width as the adhesive strength.

**Chlorophyll content measurement of the leaf after applying adhesive hydrogel.** The chlorophyll content of the plant after applying the hydrogel was evaluated with a chlorophyll meter (SPAD 502 chlorophyll meter) on devil's ivy (*Epipremnum aureum*). Devil's ivy was selected as a model plant for the chlorophyll measurement, as it has large and mechanical-insensitive leaves for chlorophyll meter clipping, while its leaf texture and thickness are similar to a Venus flytrap. Briefly, a hydrogel film ( $0.5 \text{ cm} \times 0.5 \text{ cm}$ ) with a PDMS cover was attached on the leaf of devil's ivy; the chlorophyll content was measured every 1 h for 10 h. Totally, six leaves were examined with the chlorophyll meter.

**On-plant impedance measurement.** The impedance between the two conformable electrodes on the plant surface was measured as the on-plant impedance. Aloe vera was used as a model plant to test the on-plant impedance. A flytrap usually presents thin and irregular petioles, making it difficult to directly measure the on-plant impedance with a standardized protocol. On the other hand, aloe vera shows large surfaces; different electrodes can be applied to it with the same measurement protocols. Briefly, the surface of one aloe vera stem was cleaned with a Kimwipe; then conformable electrodes with a predefined area of  $1 \text{ cm} \times 1 \text{ cm}$  were attached to the aloe vera surface separated by 1 cm. The impedance between the two electrodes was measured by an electrochemical workstation (Zennium E, Zahner Ennium) in the frequency range from  $10^0$  to  $10^6$  Hz. After the measurement of the conformable electrodes, the electrodes were peeled off and cleaned with Kimwipe again; then Ag/AgCl–agar electrodes were placed in the same position. The same settings were used for the Ag/AgCl–agar on-plant impedance measurement.

**Mechanical stimulation of the flytrap.** Flytraps were purchased from ANR Technologies in Singapore. All the flytraps were grown from tissue culture. Two conformable electrodes ( $3 \text{ mm} \times 3 \text{ mm}$ ) were attached to the flytrap in a pot.

One conformable electrode was attached to the centre of the lower epidermis of the flytrap as a recording electrode (positive terminal); the other conformable electrode was attached to the petiole surface of the flytrap as a reference electrode (negative terminal). One mechanosensitive hair of the flytrap was gently hovered by a wooden stick. The mechanosensitive hair was stimulated every 100 s, which confirmed the generation of a series of APs every 100 s, but they did not close the flytrap lobes. The electrical signals were measured using a homemade Faraday cage. The two terminals were connected to the analogue inputs of a data acquisition system (USB-2610 series, Smaqc Technologies) in the Faraday cage without using a low-pass filter. There are no observable high-frequency noises in the measured signals. The data acquisition system was operated in the differential mode to reject common-mode noises and was sampled at the rate of 100 Hz. The sampling rate was verified as shown in Supplementary Fig. 15. The ground terminal of the data acquisition system was connected with the Faraday cage for the shielding of electromagnetic interference.

**Electrical stimulation of the flytrap.** Four conformable electrodes (two pairs, 3 mm × 3 mm each) were attached to the lower epidermis of the flytrap lobe (Fig. 2a). For the applied voltage pair, the positive terminal was attached near the midrib and the negative terminal was attached to the centre of the lobe. For the potential signal measurement pair, the positive terminal was attached to the centre of the lobe and the negative terminal was attached near the midrib. For d.c. stimulation, the applied voltage pair was connected to a Keithley sourcemeter (Keithley 2450). The current was simultaneously measured using the Keithley sourcemeter while applying the voltage stimulation. For frequency-dependent stimulation, the applied voltage pair was connected to a function generator (Keysight Technologies 33210A). Further, 3 V square waves at different frequencies (0.10, 0.25, 0.50, 1.00 and 2.00 Hz) were supplied by the function generator. The electrical signal measurement pair was connected to the analogue inputs of a data acquisition system (USB-2610 series, Smaqc Technologies) using the differential mode at a sampling rate of 100 Hz. All the measurements were conducted in a Faraday cage.

**Data processing and analysis.** The normalized flytrap lobe-edge distance ( $y/y_0$ ) was used to reflect the flytrap lobe closing process. A camera was placed in front of the flytrap under study to take a video of the flytrap closing. The video was converted into a series of images at a sampling rate of 10 frames  $s^{-1}$ . The changing flytrap lobe-edge distance ( $y$ ) was measured using the ImageJ software, and all the  $y$  values were divided by the initial lobe-edge distance before flytrap closing ( $y_0$ ). The  $y/y_0$  data were aligned with the applied voltage data or potential signal data in a time sequence to study the relationships between electrical stimulation, action potential and flytrap actuation. The response time was extracted from the  $y/y_0$  data by annotating the time of the start of electrical stimulation and the start of flytrap closing. This time interval was noted as the response time. The first two-AP interval was extracted from the potential signal data. The time points where the first and second AP-peak maxima appeared were annotated and subtracted. This time interval was noted as the first two-AP interval. The correlation between the response time and the first two-AP interval was fitted by a line without fixing the intercept or slope. The AP interval was analysed based on the AP series data of potential signals under d.c. stimulation. The time points where the AP maxima appeared were annotated, and the neighbouring time points were subtracted to determine the time intervals. The time intervals are noted as AP intervals. The normalized actuating speed of the modular flytrap from d.c. stimulation and 2 Hz stimulation were obtained by taking the first-order derivative of the  $y/y_0$  data (Supplementary Fig. 28) and the data points were connected with a B-spline.

**Fabrication of an electrically modulated phytoactuator.** The electrically modulated phytoactuator comprised the flytrap and conformable electrodes. The phytoactuator was worn on a finger and controlled by a smartphone, integrated with a robotic arm to pick up a fine wire, and integrated on a manipulator to capture moving objects. The flytrap was cut from its petiole and the cutting area was immediately sealed with Ecoflex elastomer. Two conformable electrodes (3 mm × 3 mm) were attached to the lower epidermis of one flytrap lobe. The positive terminal was attached near the midrib and the negative terminal was attached to the centre of the lobe. The two conformable electrodes were connected with the two GPIO terminals of the Wi-Fi module (ESP8266). The positive terminal was connected to an output terminal of the Wi-Fi module, and the negative terminal was connected to a ground terminal of the Wi-Fi module. The Wi-Fi module was programmed to communicate with a smartphone by a customized mobile app created using the Blynk IoT platform. The codes to program the Wi-Fi module can be found in Github (<https://github.com/Wenlong0-0/Wireless-control-of-phytoactuator>). A D-Link router was used to allow Internet access to the Wi-Fi module. The programmable bionic robotic hand ( $\mu$ hand) was purchased from VANBOT. The moving object was controlled by a customized LabVIEW (2017) motorized device.

## Data availability

The data that support the plots in this paper and other findings of this study are available from the corresponding author upon reasonable request.

## Code availability

The code to program the ESP8266 Wi-Fi module in the Blynk IoT platform is available at <https://github.com/Wenlong0-0/Wireless-control-of-phytoactuator>.

Received: 11 February 2020; Accepted: 17 December 2020;

Published online: 25 January 2021

## References

- Rus, D. & Tolley, M. T. Design, fabrication and control of soft robots. *Nature* **521**, 467–475 (2015).
- Walsh, C. Human-in-the-loop development of soft wearable robots. *Nat. Rev. Mater.* **3**, 78–80 (2018).
- Rich, S. I., Wood, R. J. & Majidi, C. Untethered soft robotics. *Nat. Electron.* **1**, 102–112 (2018).
- McEvoy, M. A. & Correll, N. Materials that couple sensing, actuation, computation, and communication. *Science* **347**, 1261689 (2015).
- Kim, Y., Parada, G. A., Liu, S. & Zhao, X. Ferromagnetic soft continuum robots. *Sci. Robot.* **4**, eaax7329 (2019).
- Li, S., Vogt, D. M., Rus, D. & Wood, R. J. Fluid-driven origami-inspired artificial muscles. *Proc. Natl Acad. Sci. USA* **114**, 13132–13137 (2017).
- Yang, H. et al. 3D printed photoresponsive devices based on shape memory composites. *Adv. Mater.* **29**, 1701627 (2017).
- Vatankhah-Varnoosfaderani, M. et al. Bottlebrush elastomers: a new platform for freestanding electroactuation. *Adv. Mater.* **29**, 1604209 (2017).
- Morimoto, Y., Onoe, H. & Takeuchi, S. Biohybrid robot powered by an antagonistic pair of skeletal muscle tissues. *Sci. Robot.* **3**, eaat4440 (2018).
- Li, Z. et al. Biohybrid valveless pump-bot powered by engineered skeletal muscle. *Proc. Natl Acad. Sci. USA* **116**, 1543–1548 (2019).
- Ricotti, L. et al. Biohybrid actuators for robotics: a review of devices actuated by living cells. *Sci. Robot.* **2**, eaq0495 (2017).
- Cai, P. et al. Biomechano-interactive materials and interfaces. *Adv. Mater.* **30**, 1800572 (2018).
- Feinberg, A. W. et al. Muscular thin films for building actuators and powering devices. *Science* **317**, 1366–1370 (2007).
- Appiah, C. et al. Living materials herald a new era in soft robotics. *Adv. Mater.* **31**, 1807747 (2019).
- Trewavas, A. Plant intelligence: mindless mastery. *Nature* **415**, 841 (2002).
- Trewavas, A. What is plant behaviour?. *Plant Cell Environ.* **32**, 606–616 (2009).
- Skrzypczak, T. et al. Plant science view on biohybrid development. *Front. Bioeng. Biotechnol.* **5**, 46 (2017).
- Baluška, F., Gagliano, M. & Witzany, G. *Memory and Learning in Plants* (Springer, 2018).
- Boudaoud, A. An introduction to the mechanics of morphogenesis for plant biologists. *Trends Plant Sci.* **15**, 353–360 (2010).
- Qi, J. et al. Mechanical regulation of organ asymmetry in leaves. *Nat. Plants* **3**, 724–733 (2017).
- Chen, H. et al. Ultrafast water harvesting and transport in hierarchical microchannels. *Nat. Mater.* **17**, 935–942 (2018).
- Barthlott, W., Mail, M., Bhushan, B. & Koch, K. Plant surfaces: structures and functions for biomimetic innovations. *Nano-Micro Lett.* **9**, 23 (2017).
- Mousavi, S. A. R., Chauvin, A., Pascaud, F., Kellenberger, S. & Farmer, E. E. *GLUTAMATE RECEPTOR-LIKE* genes mediate leaf-to-leaf wound signalling. *Nature* **500**, 422–426 (2013).
- Markin, V. S., Volkov, A. G. & Jovanov, E. Active movements in plants. *Plant Signal Behav.* **3**, 778–783 (2008).
- Scherzer, S., Federle, W., Al-Rasheid, K. A. S. & Hedrich, R. Venus flytrap trigger hairs are micronewton mechano-sensors that can detect small insect prey. *Nat. Plants* **5**, 670–675 (2019).
- Hedrich, R. & Neher, E. Venus flytrap: how an excitable, carnivorous plant works. *Trends Plant Sci.* **23**, 220–234 (2018).
- Volkov, A. G., Adesina, T. & Jovanov, E. Closing of Venus flytrap by electrical stimulation of motor cells. *Plant Signal Behav.* **2**, 139–145 (2007).
- Volkov, A. G., Adesina, T. & Jovanov, E. Charge induced closing of *Dionaea muscipula* Ellis trap. *Bioelectrochemistry* **74**, 16–21 (2008).
- Grimnes, S. & Martinsen, Ø. G. *Bioimpedance and Bioelectricity Basics* 3rd edn, (Elsevier, 2015).
- Volkov, A. G. *Plant Electrophysiology: Theory and Methods* (Springer, 2006).
- Salvador-Recatalá, V., Tjallingii, W. F. & Farmer, E. E. Real-time, in vivo intracellular recordings of caterpillar-induced depolarization waves in sieve elements using aphid electrodes. *N. Phytol.* **203**, 674–684 (2014).
- Volkov, A. G. et al. Memory elements in the electrical network of *Mimosa pudica* L. *Plant Signal Behav.* **9**, e982029 (2014).
- Mousavi, S. A. R., Nguyen, C. T., Farmer, E. E. & Kellenberger, S. Measuring surface potential changes on leaves. *Nat. Protoc.* **9**, 1997–2004 (2014).
- Kim, J. J., Allison, L. K. & Andrew, T. L. Vapor-printed polymer electrodes for long-term, on-demand health monitoring. *Sci. Adv.* **5**, eaaw0463 (2019).

35. Naficy, S., Razal, J. M., Whitten, P. G., Wallace, G. G. & Spinks, G. M. A pH-sensitive, strong double-network hydrogel: poly(ethylene glycol) methyl ether methacrylates–poly(acrylic acid). *J. Polym. Sci. B* **50**, 423–430 (2012).
36. Ramanath, G. et al. Templateless room-temperature assembly of nanowire networks from nanoparticles. *Langmuir* **20**, 5583–5587 (2004).
37. Ho, M. D., Liu, Y., Dong, D., Zhao, Y. & Cheng, W. Fractal gold nanoframework for highly stretchable transparent strain-insensitive conductors. *Nano Lett.* **18**, 3593–3599 (2018).
38. Trebacz, K. & Sievers, A. Action potentials evoked by light in traps of *Dionaea muscipula* Ellis. *Plant Cell Physiol.* **39**, 369–372 (1998).
39. Volkov, A. G., Adesina, T., Markin, V. S. & Jovanov, E. Kinetics and mechanism of *Dionaea muscipula* trap closing. *Plant Physiol.* **146**, 694–702 (2008).
40. Miyamoto, A. et al. Inflammation-free, gas-permeable, lightweight, stretchable on-skin electronics with nanomeshes. *Nat. Nanotechnol.* **12**, 907–913 (2017).
41. Yuk, H., Lu, B. & Zhao, X. Hydrogel bioelectronics. *Chem. Soc. Rev.* **48**, 1642–1667 (2019).
42. Liu, Y. et al. Soft and elastic hydrogel-based microelectronics for localized low-voltage neuromodulation. *Nat. Biomed. Eng.* **3**, 58–68 (2019).
43. Stavrinidou, E. et al. Electronic plants. *Sci. Adv.* **1**, e1501136 (2015).
44. Wong, M. H. et al. Nitroaromatic detection and infrared communication from wild-type plants using plant nanobionics. *Nat. Mater.* **16**, 264–272 (2016).
45. Stavrinidou, E. et al. In vivo polymerization and manufacturing of wires and supercapacitors in plants. *Proc. Natl Acad. Sci. USA* **114**, 2807–2812 (2017).

## Acknowledgements

We acknowledge financial support from the National Research Foundation (NRF), Prime Minister's Office, Singapore, under its NRF Investigatorship (NRF-NRFI2017-07) and the Agency for Science, Technology and Research (A\*STAR) under its AME Programmatic Funds (project no. A18A1b0045) on Cyber-Physiochemical Interfaces (CPI) Programme. N.M. was supported by the Japan Society for the Promotion of Science (JSPS) overseas

research fellowship. Finally, we thank A. L. Chun for critically reading and editing the manuscript.

## Author contributions

W.L., N.M. and X.C. designed the project and experiments. Zhiyuan Liu assisted with the conformable electrode design, fabrication and characterization. W.L. and M.W. synthesized and characterized the adhesive hydrogel. Y.L. and W.L. prepared the cross-section of the plant and hydrogel for the optical microscope. P.C. assisted with the fabrication of the conformable electrode. G.C. and W.L. designed and performed the adhesive strength measurement of the electrode. W.L., F.Z. and C.L. performed the flytrap electrical signal measurement, flytrap mechanical and electrical stimulation, and phytoactuator implementation. Zhihua Liu designed and manufactured the LabVIEW-controlled motorized device for the accurate capture of moving objects. Z.Lv and W.L. fabricated the AgNW and CNT conductors. W.Z. performed the transmission electron microscopy investigation for the Au nanomesh. W.L., N.M. and X.C. wrote the manuscript. All the authors read and revised the manuscript.

## Competing interests

The authors declare no competing interests.

## Additional information

**Supplementary information** is available for this paper at <https://doi.org/10.1038/s41928-020-00530-4>.

**Correspondence and requests for materials** should be addressed to X.C.

**Peer review information** *Nature Electronics* thanks Ingrid Graz, Alexander Volkov and the other, anonymous, reviewer(s) for their contribution to the peer review of this work.

**Reprints and permissions information** is available at [www.nature.com/reprints](http://www.nature.com/reprints).

**Publisher's note** Springer Nature remains neutral with regard to jurisdictional claims in published maps and institutional affiliations.

© The Author(s), under exclusive licence to Springer Nature Limited 2021